Nanoscale Res Lett
DOI 10.1007/s11671-007-9058-4

NANO EXPRESS

Effect of surrounding environment on atomic structure and equilibrium shape of growing nanocrystals: gold in/on SiO_2

F. Ruffino · C. Bongiorno · F. Giannazzo · F. Roccaforte · V. Raineri · M. G. Grimaldi

Received: 21 March 2007 / Accepted: 13 April 2007

Abstract We report on the equilibrium shape and atomic structure of thermally-processed Au nanocrystals (NCs) as determined by high resolution transmission electron microscopy (TEM). The NCs were either deposited on SiO_2 surface or embedded in SiO_2 layer. Quantitative data on the NCs surface free energy were obtained via the inverse Wulff construction. Nanocrystals inside the SiO_2 layer are defect-free and maintain a symmetrical equilibrium shape during the growth. Nanocrystals on SiO_2 surface exhibit asymmetrical equilibrium shape that is characterized by the introduction of twins and more complex atomic defects above a critical size. The observed differences in the equilibrium shape and atomic structure evolution of growing NCs in and on SiO_2 is explained in terms of evolution in isotropic/anisotropic environment making the surface free energy function angular and/or radial symmetric/asymmetric affecting the rotational/translational invariance of the surface stress tensor.

Keywords Nanocrystal · Crystal growth · Transmission electron microscopy · Wulff plot · Surface energy · Gold · SiO_2

F. Ruffino · M. G. Grimaldi
MATIS CNR-INFM and Dipartimento di Fisica e Astronomia, Università di Catania, via S. Sofia 64, 95123 Catania, Italy

F. Ruffino (✉) · C. Bongiorno · F. Giannazzo · F. Roccaforte · V. Raineri
Consiglio Nazionale delle Ricerche – Istituto per la Microelettronica e Microsistemi (CNR-IMM), Stradale Primosole 50, 95121 Catania, Italy
e-mail: francesco.ruffino@ct.infn.it

Introduction

The discovery of nanostructures (quantum dots, nanoparticles, quantum wires, nanowires, etc.) have stimulated research in many different areas, becoming the basis for the ''Nano-electronic and Nano-technology revolution'' [1–3]. The fundamental issue of such a revolution is the effort towards the fabrication of innovative nano-structured functional materials and, in particular, the acquisition of the capability to control all their characteristics (electrical, optical, mechanical, etc.) by the atomic-level manipulation of the structural ones.

In particular, nano-structured materials fabricated by metal nanocrystals (NCs) dispersed in or deposited on insulator matrices have been extensively studied [4–7] because their unique optical, magnetic and electrical properties and thanks to the possibility of control such properties in a wide range simply controlling the NCs structural properties (atomic structure, size, density, etc.). It is well-known that the NCs characteristics are size-dependent and intermediate between the properties of the atomic and bulk matter [4, 8]: such a peculiar property results from the NCs nanometric dimensions and in particular from the enhanced surface-area-to-volume ratio (with respect to the bulk matter) and thus vary as a function of NC size (as a consequence of the limited number of atoms incorporated therein and the considerable influence of surface atoms) [9]. For these reasons, nano-structured materials based on metal NCs acquired a relevant role for the design and fabrication of nano-devices with numerous applications ranging from micro- and nano-electronics to catalysis, gas sensor, biology and many others. On the other hand, in view of the fabrication of innovative nano-devices using metal NCs in/on insulator substrates with pre-determined tunable (electrical, optical,...) properties, it

is fundamental to know the details of the chemical and physical interaction between the NCs and the surrounding environment to understand (and to control) the structural ones and their evolution as a function of the NCs size.

In the present work, we study the influence of the surrounding environment on the atomic structure and equilibrium shape of growing NCs focusing on Au NCs/SiO_2 system. We choose such a system because its potential application in the fabrication of nano-electronic, opto-electronic (plasmonics) and gas-sensor innovative devices [10–12]. On the other hand, exists from 80s a vast experimental and theoretical literature concerning the study of free and supported Au NCs [9, 13–24]. The experimental works are primarily based on the study of the Au NCs structure and equilibrium shape by transmission electron microscopy (TEM), while the theoretical ones on simulation of the atomic structures and equilibrium shapes by several models (Monte-Carlo, Density functional theory). The present work, gives a contribution to the experimental investigation evidencing clear differences (by TEM analyses) in the atomic structure and equilibrium shape of growing Au NCs embedded in SiO_2 layers from those supported on SiO_2 and can furnish new theoretical basis to include the effect of the environment surrounding the NCs in the simulation models. An explanation of the observed differences in terms of thermodynamic concepts and symmetry considerations is given. In particular, we demonstrate how to extract quantitative information about the surface free energy of the Au NCs grown in and on SiO_2 using the inverse Wulff construction basing on the equilibrium shape inferred by high-resolution transmission electron microscopy (HR-TEM). Furthermore, the method to growth ideal NCs on surfaces come out and the conclusions can be extended to other crystalline nanoclusters of other materials.

Experiment

To avoid any possible difference in the Au NCs structures and shapes as a consequence of differences in samples preparation, we followed a unique procedure to prepare the samples with NCs inside and over amorphous SiO_2. CZ- <100> silicon substrates with resistivity $\rho \approx 6 \times 10^{-3}$ Ω cm were etched in a 10% aqueous HF solution to remove the native oxide, and subsequently annealed at 1223 K for 15 min in O_2 in order to grow an uniform, 10 nm thick, amorphous SiO_2 layer (as determined by ellypsometric measurements and subsequent cross-sectional TEM). A 2 nm thick Au film was deposited (at room temperature) by sputtering on the SiO_2 layer using an Emitech K550x Sputter coater apparatus (Ar plasma, 10^{-4} Pa pressure). In some samples the Au layer was covered by a 3 nm thick SiO_2 layer deposited (at room temperature) by sputtering using an AJA RF Magnetron sputtering apparatus (Ar plasma, 1.3×10^{-8} Pa pressure). Then, the Au/SiO_2 and SiO_2/Au/SiO_2 samples were contemporary annealed in Ar ambient in the 873–1073 K temperature range and in the 5–60 min time range to obtain the NCs self-organization and growth.

The samples were analyzed by Rutherford backscattering spectrometry (RBS), TEM and HR-TEM, after mechanical polishing and final Ar ion milling. The RBS analyses were performed using 2 MeV $^4He^+$ backscattered ions at 165°. The TEM analyses were performed by a Jeol 2010F energy filtered transmission microscope (EFTEM), operating at 200 kV and equipped with a Gatan image filtering apparatus. EFTEM allowed to map of the elemental composition of the samples with spatial resolution typical of TEM analyses, by selecting electrons with a well defined energy from the transmitted beam. Before the cross-sectional TEM analyses of the samples with Au on SiO_2, a thin SiO_2 cap-layer (~3 nm) was deposited (by sputtering with the AJA RF Magnetron apparatus) on the samples in order to protect the NCs during the samples preparation. It is worth to note that this last deposition was performed at room temperature, so that we can assume that the Au NCs do not change their atomic structure and equilibrium shape in consequence of the SiO_2 protective-layer deposition because it is quite improbably that they release energy during such a process.

Results

Rutherford backscattering spectrometry analyses allowed to determine the deposited Au atomic surface density Q: for all the samples (Au in and on SiO_2, as-deposited and annealed) it is the same (within a statistical error of 5%) and equal to $Q \approx 9 \times 10^{15}$ Au/cm^2. So, we can conclude that no Au loss occurs during thermal treatments (evaporation, out-diffusion).

Plan- and cross-sectional TEM analyses allowed to follow the evolution of the NCs size distribution as a function of annealing temperature and time. As an example, Fig. 1 shows plan-view TEM images for some annealed samples. Figure 1a and b refer to the samples annealed at 873 K for 20 min but with Au NCs within and over the SiO_2 layer, respectively. Figure 1c and d show the images for the Au NCs in and on SiO_2 annealed at 1073 K for 60 min. The inset of each figure shows the derived NCs size distribution, reproduced by a Gaussian fit (continuous line), and the relative mean radius $<R>$, derived as the position of the Gaussian peak. The error on $<R>$ was evaluated as the standard deviation σ (1/2 of the full width at half maximum) of the Gaussian fit. The systematic

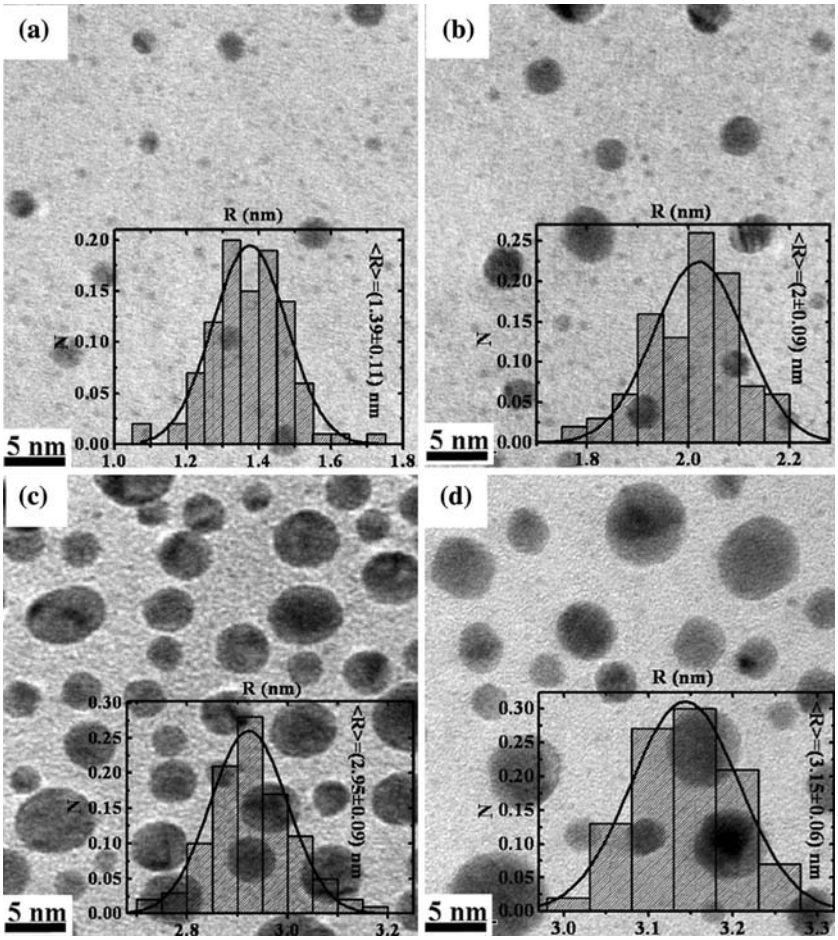

Fig. 1 Plan-TEM images of the samples (**a**) with Au NCs inside the SiO_2 layer and annealed 873 K–20 min, (**b**) with Au NCs over the SiO_2 layer and annealed 873 K–20 min, (**c**) with Au NCs inside the SiO_2 layer and annealed 1073 K–60 min, (**d**) with Au NCs over the SiO_2 layer and annealed 1073 K–60 min. The inset of each figures show the obtained NCs radius distribution (N is the normalized number of NCs and R the NCs radius, <*R*> the mean NC radius)

behavior observed consists in an increase of the mean NCs radius (translation of the radius distribution towards higher sizes) and a decrease of σ (narrowing of radius distribution) when annealing temperature and/or time are increased. The systematic analyses of the evolution of such a distribution as a function of annealing temperature and time allowed to elucidate the kinetic growth mechanism (in the analyzed annealing temperature and time range) of the Au NCs in and on SiO_2 in a ripening process of three-dimensional structures limited by diffusion but with different growth rates. In particular, a lower growth rate for the NCs embedded in SiO_2 was found with respect to the growing NCs on SiO_2 as evident from the TEM images and distributions in Fig. 1 (and considering that the starting distributions for the NCs in and on SiO_2 are identical). In particular, we determined the increase of the mean radius <*R*> from (1.24 ± 0.16) nm to (2.95 ± 0.09) nm for the Au NCs in SiO_2 and to (3.15 ± 0.06) nm for those supported on SiO_2 (in the same range of annealing temperature and time). The detailed study of the kinetic growth mechanisms of Au NCs on SiO_2 are reported by Ruffino et al. [25] and for the Au NCs in SiO_2 by De Marchi et al. [26] and Miotello et al. [27].

NCs internal structures and morphologies were examined using Fresnel contrast and HR-TEM analyses. The first result was obtained by analyses on significant statistical population of NCs (were analyzed 100 NCs for each sample): their internal atomic structures and shapes are determined only by their size and not by the particular annealing process performed. This fact means that each sample is characterized by a distribution of NCs size (which mean value increases when annealing temperature and time increase) but in all the samples with Au NCs inside SiO_2, independently from the temperature, the smaller NCs have a similar structure between them, the greater NCs are a similar structure between them but different with respect to the smaller ones. The same situation occurs for the NCs over SiO_2 but in a different manner from those grown inside the SiO_2 layer. In particular, for the Au NCs embedded in SiO_2, the HR-TEM images indicate that, in the range of radius 1 nm < R < 3.5 nm the NCs always exhibit a single-crystal-icosahedral structure (close-packing of atoms structure) [14] free of internal defects as indicated by the representative HR-TEM images in Fig. 2a, b and c (more complex different structures, such as Marks decahedra or cuboctahedra, are evident for higher

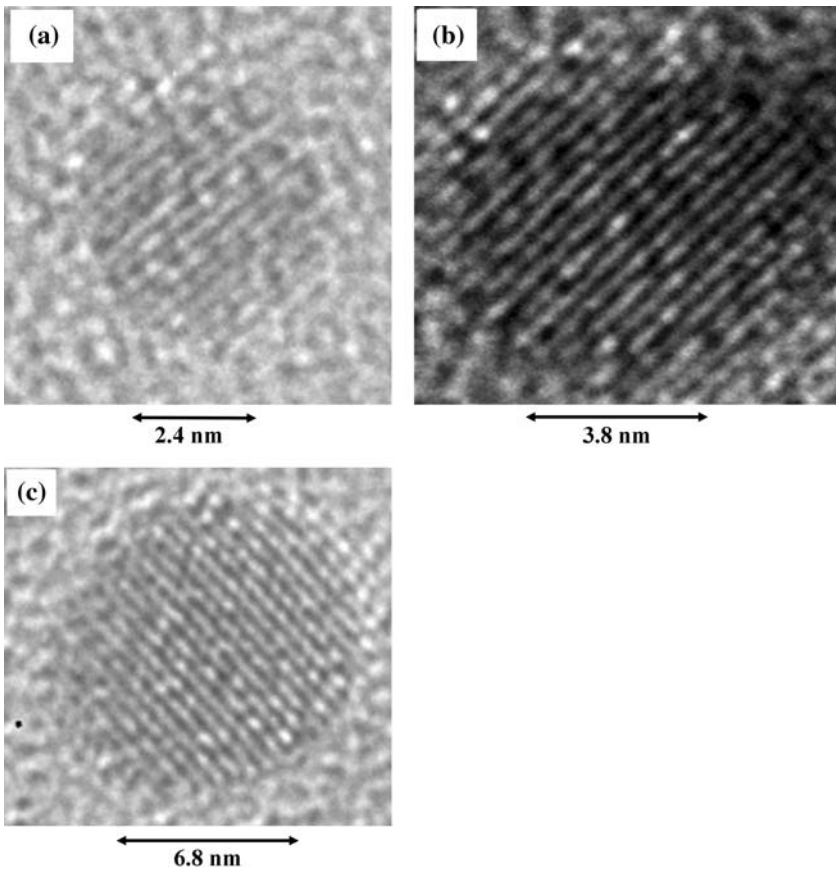

Fig. 2 HR-TEM images of Au NCs in SiO_2 with the same size as the NCs on SiO_2 forming the three determined groups

sizes). These images refer to the samples as-deposited (a), annealed 873 K–60 min (b) and 1073 K–60 min (c), respectively. They show a good resemblance with the proposed model for Au NCs structure viewed along (110) [13]. The spacing between the crossing (111) planes is 0.235 nm in this projection and the Au-Au distance is 0.25 nm. The fact that all the NCs in SiO_2, with size in this range, exhibit single-crystal-icosahedral structure, free of internal defects reflects a situation in which their equilibrium shape symmetry is conserved when they grow.

Also the HR-TEM images of the NCs deposited and annealed over SiO_2 show a good resemblance with the proposed model for Au NCs structure viewed along (110) but, differently from the NCs growing in SiO_2, the data seem to delineate three large groups of structures, determined by the NCs size (in the same size range 1 nm < R < 3.5 nm):

- Group 1 (a representative NC in Fig. 3a): it is formed by NCs with a radius $R < 1.5$ nm; they have single-crystal-icosahedra structure [14] free of internal defects;
- Group 2 (representative NC in Fig. 3b) it is formed by NCs with a radius 1.5 nm $< R < 2$ nm; they have a (111)-twinned icosahedral structure [14];
- Group 3 (representative NC in Fig. 3c): it is formed by NCs with a radius 2 nm $< R <$ 3.5 nm; they have a complicate decahedral multi-twinned (and lamellar) structure [14].

From the representative images reported in Fig. 3 (that refer to the samples as-deposited (a), annealed 873 K–60 min (b) and 1073 K–60 min (c), respectively) it is clear that the evolution in size of the supported NCs on SiO_2 corresponds to an evolution of the equilibrium shape with a progressive loss of symmetry and a corresponding introduction of internal defects. In this figure, were reported representative images of NCs with size similar to those reported in Fig. 2 to make a direct comparison: the NC in Fig. 3a (representative of the group 1 of growing NCs on SiO_2) has an atomic structure (single icosahedral) coincident with those showed in Fig. 2a, b and c (growing NCs in SiO_2); images in Fig. 3b and c show NCs representative of the growing NCs on SiO_2 belonging to the group 2 and 3, respectively: it is evident the different atomic structure in comparison with the NCs grown in SiO_2 and with similar sizes (Fig. 2b and c). The NCs of group 2, despite the similar single-crystal-icosahedral structure as the NCs of group 1, are characterized by the introduction of twins of (111) planes corresponding to introduction of asymmetry in the NC shape. For the NCs of group 3 occurs a transition from the icosahedral structure to the decahedral

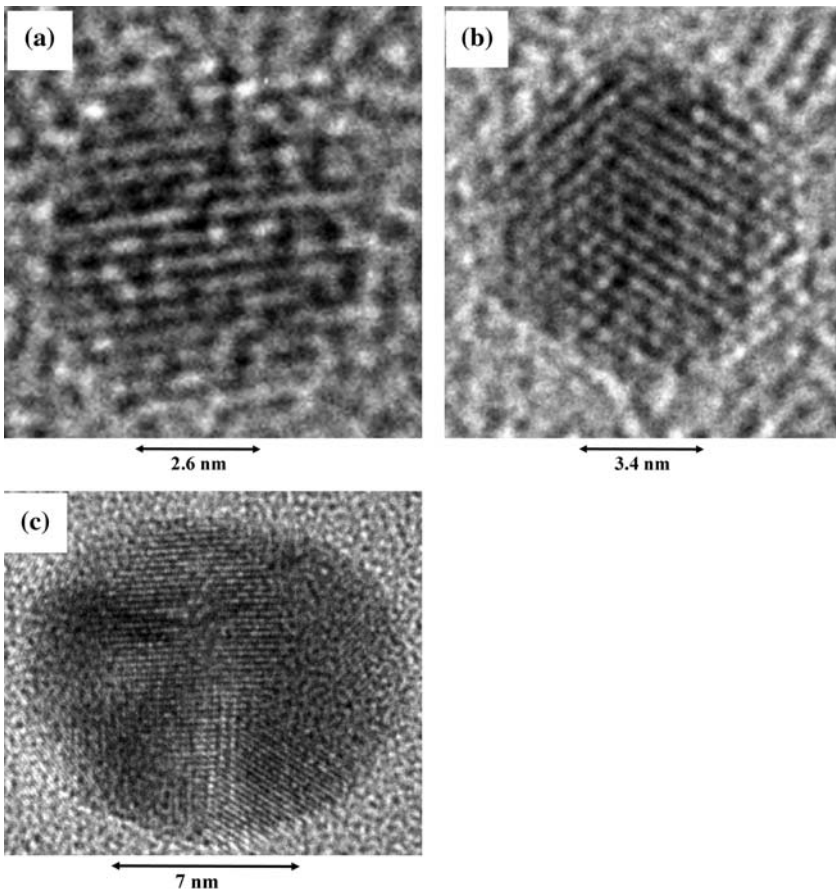

Fig. 3 HR-TEM images of Au NCs on SiO_2 for the three determined groups ((**a**) relative to the group 1, (**b**) to the group 2 and (**c**) to the group 3)

one, characterized by the introduction of multi-twins and completely lost shape symmetry.

Discussion

To explain the differences observed in the atomic structure and equilibrium shape of Au NCs with similar size but grown inside and over the amorphous SiO_2 layer, in this section we illustrate a discussion based on thermodynamic and symmetry considerations. In particular, we base our discussion on the concept of angular and radial symmetry/asymmetry of the NC surface free energy corresponding to a symmetrical/asymmetrical spatial situation of the environment surrounding the NC. Furthermore, we correlate the angular/radial symmetric/asymmetric behaviour of the NC surface free energy with the rotational/translational invariance of the surface stress tensor of the NC.

In the bulk form Au has the face centred cubic (FCC) structure which is closest packed. As a consequence Au macro-crystals exhibit the symmetric cubic, octahedral or rhombododecahedral crystal form associated with the FCC structure. For the Au NCs the situation is more complicated because the strongly influence of the surface atoms. The FCC Au based NCs generally present to the environment as a combination of crystal facets of the {111} and {100} planes in icosahedral or decahedral structure that yield to an efficient compromise between surface area and packing [28]. It is known, furthermore, that the surface of Au shows a tendency to reconstruct so that the surface atoms are closely packed together [29]. This behaviour could be due to the relief of large tensile surface stress in the unreconstructed surface. The most striking reconstruction was observed in the (111) plane [30] (that is expected to be the closest packing plane, the plane with the lowest surface free energy). Such a plane forms a $23 \times \sqrt{3}$ reconstruction which appears to involve the insertion of an extra row of atoms into the surface every 23 rows [31]. This reconstruction clearly decreases the average coordination number of the atoms because to form it atoms must be taken from 12-fold-coordinated bulk sites placed in 9-fold-coordinated surface sites. Such a reconstruction could only be lower in energy than the unreconstructed surface if the shorter bond-lengths that are formed in the plane of the surface are energetically favourable. Then, the unreconstructed Au (111) surface exhibit a considerable tensile surface stress and the driving force for the $23 \times \sqrt{3}$ reconstruction is the relief of this tensile surface stress.

In our discussion, we, according to Shuttleworth [32] and Cammarata [33], define the second rank surface stress tensor f_{ij} of the NC by:

$$f_{ij} = \gamma\delta_{ij} + \frac{\partial\gamma}{\partial\varepsilon_{ij}} \quad (1)$$

being γ the surface free energy (per unit area) of the NC, ε_{ij} the surface elastic strain tensor, δ_{ij} the Kronecker delta.

Then, we extracted quantitative data on the surface free energy from the NCs shapes via the inverse Wulff construction [34]: first, we identified the ''Wulff point'' of the NC and then applied the Wulff construction in reverse order to obtain the surface energy plot to within a constant scale factor. The Wulff point (''center of mass'') of a NC was defined as the intersection point between the perpendicular bisectors of two (111) facets. This point was taken as the centre of a polar plot, with angular and radial coordinates θ and r. For each θ_i (with a 5° spacing), we measured the distance r_i between the Wulff point and the NC surface (determined by the accurate analyses of the HR-TEM images). According to the Wulff relation $\gamma_i / r_i = \lambda = const$, the value of the surface free energy $\gamma_i \equiv \gamma(\theta_i)$ for those orientations was obtained. In this way the $\gamma(\theta)$ plot was determined. In particular, to make a direct comparison between the NCs on and in SiO_2, we distinguished the NC surface in two parts. We draw the line passing through the Wulff point and parallel to the substrate plane (using, in particular, cross-TEM images). For the NCs on SiO_2, the NCs surface above this line was defined as the surface exposed to the Ar (the gas environment in which were performed the annealing processes), while the below one as the surface exposed to SiO_2. In the same way for the NCs in SiO_2, but considering that the upper and lower parts of surface are anywhere exposed to SiO_2. According to this consideration, we named $\gamma_{up}(\theta)$ the NC surface energy relative to the upper surface part and $\gamma_{down}(\theta)$ the NC surface energy relative to the bottom part, so that for the NCs on SiO_2 is $\gamma_{up}(\theta) \equiv \gamma_{Au/Ar}(\theta)$ and $\gamma_{down}(\theta) \equiv \gamma_{Au/SiO_2}(\theta)$ (θ), while for the NCs in SiO_2 is $\gamma_{up}(\theta) \equiv \gamma_{Au/SiO_2}(\theta)$ and $\gamma_{down}(\theta) \equiv \gamma_{Au/SiO_2}(\theta)$.

For each class of NCs shapes (Fig. 2 and Fig. 3), an averaged $\gamma(\theta)$ plot is shown in Fig. 4 and Fig. 5, where the relative energies are normalized to the surface free energy for the (111) plane. For all the plots the zero in the angle scale was taken as the direction of one (111) plane of the NC. However, the r_i values for each θ_i are averaged over 10 different NCs belonging to the same group (i.e. similar size). The NC-to-NC variation in $\gamma(\theta)$ for a given orientation was indicated as the error bars reported in Fig. 4 and 5.

First we consider the case of Au NCs in SiO_2: from Fig. 4a, it is clear that the peaks and valleys in the $\gamma_{up}(\theta)$

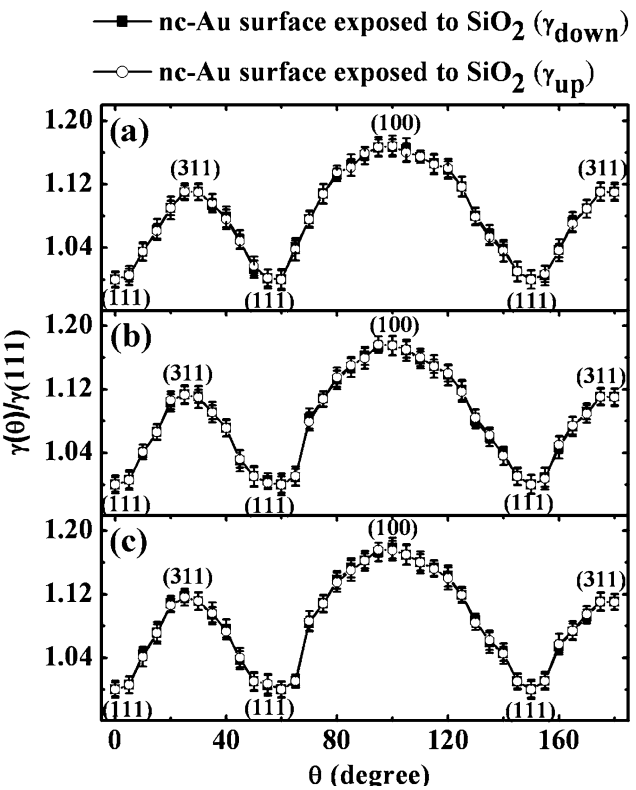

Fig. 4 Wulff plot ($\gamma_{up}(\theta) = \gamma_{Au/SiO_2}(\theta)$ and $\gamma_{down}(\theta) = \gamma_{Au/SiO_2}$) for the NCs in SiO_2, with the same size as the NCs on SiO_2 forming the three determined groups

and $\gamma_{down}(\theta)$ lie in identical angular position (angular symmetry of $\gamma(\theta)$) and assume identical values. The latter point means that the facets with the same Miller indexes in the upper and lower parts of the NC, respectively, have identical radial coordinates (radial symmetry of $\gamma(\theta)$). Both the angular and radial symmetry of $\gamma(\theta)$ are conserved with increasing the cluster size in the cases of NCs in SiO_2, as it is evident from the comparison of Fig. 4a, b and c. This fact is reflected in the invariance of f_{ij} both for translational and rotational transformations and, as a consequence, in the symmetrical single crystal icosahedral structure for the equilibrium shape of NCs in SiO_2. Those NCs grow subjected always only to the thermodynamic process determined by the Au/SiO_2 interface in any direction, i.e. in an ''isotropic spatial situation''.

Now we consider the case of Au NCs on SiO_2. Fig. 5a shows, for the smaller sizes (group 1), a situation similar to the case of NCs in SiO_2, i.e. $\gamma_{up}(\theta)$ and $\gamma_{down}(\theta)$ lying in identical angular position and assuming identical values ($\gamma_{up}(\theta) \equiv \gamma_{Au/Ar}(\theta) \approx \gamma_{down}(\theta) \equiv \gamma_{Au/SiO_2}$) : both angular and radial symmetry of $\gamma(\theta)$ is present (f_{ij} is again invariant both for translational and rotational transformations). However, differently from the NCs in SiO_2, for sizes relative to the group 2, the angular symmetry of $\gamma(\theta)$ is still conserved, but the radial one begins to be lost

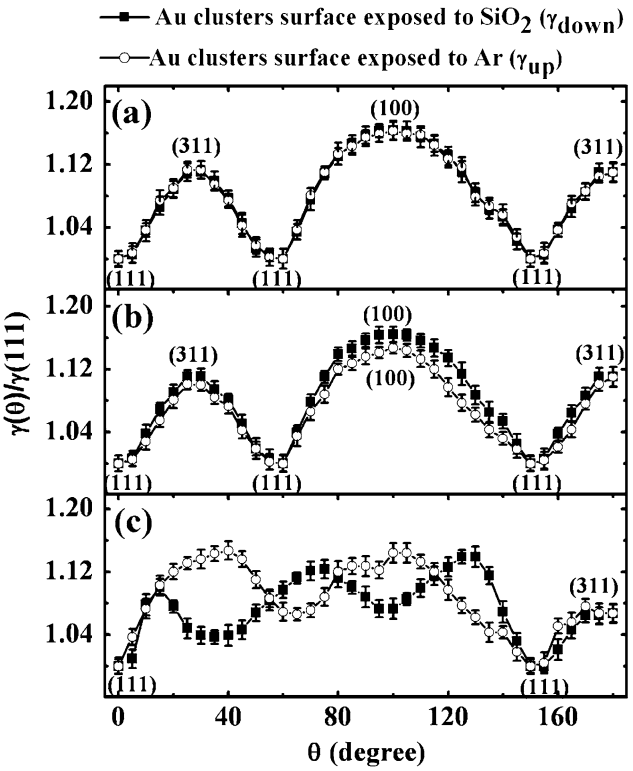

Fig. 5 Wulff plot ($\gamma_{up}(\theta) = \gamma_{Au/Ar}(\theta)$ and $\gamma_{down}(\theta) = \gamma_{Au/SiO_2}$) for the three groups of NCs on SiO_2 ((**a**) relative to the group 1 and representative NC in Fig. 3a, (**b**) to the group 2 and representative NC in Fig. 3b, (**c**) to the group 3 and representative NC in Fig. 3c)

($\gamma_{up}(\theta) \equiv \gamma_{Au/Ar}(\theta) \neq \gamma_{down}(\theta) \equiv \gamma_{Au/SiO_2}$), i.e. f_{ij} is invariant for rotational transformation but not for the translational ones. In fact, the NCs growing on SiO_2 are subjected to two thermodynamic competitive processes, due to the different surface energies of the Au/Ar interface ($\gamma_{up}(\theta) = \gamma_{Au/Ar}(\theta)$) and of the Au/$SiO_2$ interface ($\gamma_{down}(\theta) = \gamma_{Au/SiO_2}$). This is reflected in a progressive loss of symmetry in the NCs equilibrium shape with increasing the cluster radius beyond a ''critical radius'' of about 3 nm. In particular, both the angular and radial symmetry of γ (θ) are lost for the NCs of group 3 (Fig. 3c), where any correspondence between γ_{up} (θ) and γ_{down} (θ) is not present (both the rotationally and translationally invariance of the f_{ij} are lost). Furthermore, the different surface energies at Au/Ar and Au/SiO_2 interfaces determine during the NCs growth an internal strain accumulation, which is released in the formation of internal defects for larger sizes as indicated by Müller and Kern [35].

Obviously, our data are consistent with the expectation that FCC nano-structured Au present to the environment in icosahedral or decahedral structure with the {111 } planes being the closest packing planes with the lowest surface free energy. On the other hand, previous calculations [35–37] showed that for noble metals, such as Au, the ratio of the surface energies $\gamma(100)/\gamma(111)$ is close to the value of the broken-bound rule considering only the next-neighbor broken bonds. For the (111) Au there are three broken bounds for each surface atom and four for each atom of the (100), so that should be $\gamma(100)/\gamma(111) = 2/\sqrt{3} \approx 1.155$. Our data (for example in Fig. 4a) give γ (100)/γ (111) $\approx 1.167 \pm 0.018$, in good agreement with this prediction.

Finally, it is worth to note that, simply by our TEM analyses, we are not to able to correlate experimentally the NC's surface/interface energy with its surface/interface atomic density. However, the link between the surface/interface energy and the surface/interface atomic density of the NCs is possible within the theoretical framework proposed by Qi et al. [38]. Such an approach request the determination of the size-dependent cohesive energy of the NCs. The data concerning this determination and the link between the surface/interface energy and the surface/interface atomic density of the NCs by this theoretical framework will be the topic of a next specific paper.

Conclusion

We studied the effect of the surrounding environment on the atomic structure and equilibrium shape of growing NCs, considering the particular case of Au NCs in/on amorphous SiO_2. Starting from HR-TEM analyses, quantitative data on the surface free energy of the NCs were extracted by the inverse Wulff construction. The main result is that growing NCs surrounded by an ''isotropic'' environment exhibit an angular and radial symmetrical surface free energy function γ (θ) making rotationally and translationally invariant the surface stress tensor f_{ij} of the NC: this situation determines a symmetrical equilibrium shape of the NCs. Growing NCs in a ''non-isotropic'' environment exhibit a γ (θ) that lost its angular and radial symmetry for sufficiently large sizes determining the loss of the rotationally and translationally invariance of the f_{ij} and, as a consequence, a loss of symmetry in the equilibrium shape of the NC and the formation of internal defects.

The results suggest that ideal crystalline nanoclusters can be grown on surfaces simply controlling the surrounding environment even by deposition of thin layers of materials as the bulk surface.

References

1. P. Moriarty, Rep. Prog. Phys. **64**, 297 (2001)
2. D. Goldhaber-Gordon, M. S. Montemerlo, J. C. Love, G. J. Opiteck, J. C. Ellenbogen, Proc. IEEE **85**, 521 (1997)
3. D. K. Ferry, S. M. Goodnick, Transport in nanostructures (Cambridge University Press 1997)

4. Nanoparticles, edited by G. Schmid, Wiley-VCH, 2004
5. C.T. Campbell, Surf. Sci. Rep. **27**, 1(1997)
6. W. J. Kaiser, E. M. Logothesis, L. E. Wegner, J. Phys. C. **18**, L837 (1985)
7. R. Parthasarathy, Xiao-Min Lin, H. M. Jaeger, Phys. Rev. Lett. **87**, 186807 (2001)
8. R. L. Johnston, Atomic and molecular clusters (Taylor and Francis 2002)
9. A. S. Barnard, X. M. Lin, L. A. Curtiss, J. Phys. Chem. B **109**, 24465 (2005)
10. S. A. Maier, H. A. Atwater, J. Appl. Phys. **98**, 011101 (2005).
11. F. Ruffino, M. G. Grimaldi, F. Giannazzo, F. Roccaforte, V. Raineri, Appl. Phys. Lett. **89**, 263108 (2006)
12. H. Wohltjen, A. W. Snow, Anal. Chem. **70**, 2856 (1998)
13. L. R. Wallenberg, J. O. Bovin, G. Schmidt, Surf. Sci. **156**, 256 (1985)
14. L.D. Marks, Rep. Prog. Phys. **57**, 603 (1994)
15. K. Koga, K. Sugawara, Surf. Sci. **529**, 23 (2003)
16. P.A. Buffat , Mater. Chem. Phys. **81**, 368 (2003)
17. C.R. Henry, Prog. Surf. Sci. **80**, 92 (2005)
18. T. Irawan, I. Barke, H. Hövel, Appl. Phys. A **80**, 929 (2005)
19. C. L. Cleveland, U. Landman, T. G. Schaaf, M. N. Shafigullin, Phys. Rev. Lett. **79**, 1873 (1997)
20. D. Lovall, M. Buss, R. P. Andres, R. Reifenberger, Phys. Rev. B **58**, 15889 (1998).
21. R. N. Barnett, C. L. Cleveland, H. Häkkinen, W. D. Luedtke, C. Yannouleas, U. Landman, Eur. Phys. J. D **9**, 95 (1999)
22. N. T. Wilson, R. L. Johnston, Eur. Phys. J. D **12**, 161 (2000)
23. I. L. Garzón, M. R. Beltrán, G. González, I. Gutíerrez- González, K. Michaelian, J. A. Reyes-Nava, J. I. Rodríguez-Hernández, Eur. Phys. J. D 24, 105 (2003)
24. P.K. Jain, Struc. Chem. **16**, 421 (2005)
25. F. Ruffino, A. Canino, C. Bongiorno, F. Giannazzo, F. Roccaforte, V. Raineri, M. G. Grimaldi, J. Appl. Phys. **101**, 064306 (2007)
26. G. De Marchi, G. Mattei, P. Mazzoldi, C. Sada, A. Miotello, J. Appl. Phys. **92**, 4249 (2002)
27. A. Miotello, G. De Marchi, G. Mattei, P. Mazzoldi, C. Sada, Phys. Rev. B **63**, 075409, 2001
28. M. B. Cortie, E. Van der Lingen, Materials Forum **26**, 1 (2002)
29. M. A. Van Hove, R. J. Koestner, P. C. Stair, J. P. Biberian, L. L. Kesmodel, I. Bartos, G. A. Somerjiai, Surf. Sci. **103**, 218 (1981)
30. R. J. Needs, M. Mansfield, J. Phys. **1**, 7555 (1989)
31. R. Shuttleworth, Proc. Phys. Soc. A **63**, 445 (1950)
32. R. C. Cammarata, Mater. Sci. Eng. A **237**, 180 (1997)
33. C. Herring, Structures and Properties of Solid Surface (edited by R. G. Gomer and C. S. Smith, University of Chicago Press, 1953)
34. P. Müller, R. Kern, Appl. Surf. Sci. 1**62–163**, 133(2000)
35. H. P. Bonzel, Phys. Rep. **381**, 1 (2003)
36. I. Galanakis, G. Bihlmayer, V. Bellini, N. Papanikolaou, R. Zeller, S. Blügel, P. H. Dederichs, Europhys. Lett. **58**, 751 (2002)
37. M. Methfessel, D. Henning, M. Scheffler, Phys. Rev. B **46**, 4816 (1992)
38. W. H. Qi, M. P. Wang, M. Zhou, W. Y. Hu, J. Phys. D **38**, 1429 (2005)